acta physica slovaca vol. 49 No. 5, 795 – 803 October 1999

EMBEDDING DIAGRAMS OF THE OPTICAL GEOMETRY OF KERR BACKGROUNDS

Zdeněk Stuchlík[†‡1], **Stanislav Hledík**[†2]
[†] *Department of Physics, Faculty of Philosophy and Science, Silesian University, Bezručovo nám. 13, 746 01 Opava, Czech Republic*
[‡] *Theory Division, CERN, CH-1211, Geneva 23, Switzerland*

Received 16 June 1999, in final form 1 September 1999, accepted 3 September 1999

Embedding diagrams of the equatorial plane of Kerr black holes and naked singularities are constructed for the optical reference geometry related to the family of locally non-rotating observers. It is shown that turning points of the diagrams correspond to radii at which centrifugal force related to the optical geometry vanish. The corotating photon circular orbits above the outer horizon enter the embedding diagrams only for black holes with specific angular momentum $a^2 < 0.50566$, while the counterrotating photon circular orbits enter the diagrams for all black holes and naked singularities.

PACS: 04.70.Bw, 040.70.-s, 04.25.-g

1 Introduction

The optical reference geometry and the related concept of inertial forces [1] can be very helpful in understanding the character of black-hole and naked-singularity spacetimes. The optical space results from an appropriate conformal (3 + 1) splitting, and its geodesic structure illustrates several physically interesting properties of the spacetimes [2, 3, 4, 5, 6, 7].

Properties of the optical space can be conveniently demonstrated by embedding diagrams of its representative sections [1, 6, 8]. For example, the embedding diagrams clearly reflect the dynamical behaviour of test particles on circular orbits [2].

It is well known that in the spherically symmetric spacetimes (Schwarzschild, Ref. 1, Reissner-Nordström, Ref. 6, Schwarzschild-de Sitter and Schwarzschild-anti-de Sitter, Ref. 9) turning points of the embedding diagrams of the central (equatorial) planes of the optical geometry are located at radii corresponding to photon circular orbits, where the centrifugal force, defined in the framework of the optical geometry, vanish and reverses sign. Moreover, in the Schwarzschild and extreme Reissner-Nordström backgrounds, the limits of embeddability of the optical space into three-dimensional Euclidean space coincide with the limits on existence of spherically symmetric static configurations of uniform density [6]. In the case of the Schwarzschild spacetimes

[1]E-mail address: Zdenek.Stuchlik@fpf.slu.cz.
[2]E-mail address: Stanislav.Hledik@fpf.slu.cz.

with a non-zero cosmological constant, the inner limits of embeddability coincide with the inner limits on existence of static configurations of uniform density, but the outer limits are different due to presence of the cosmological constant [9, 10].

Therefore, it is natural to put the question, how the properties of the optical reference geometry of Kerr backgrounds are imprinted into the structure of the embedding diagrams of their equatorial plane, especially in spite of the fact that the centrifugal force does not vanish at the radii of photon circular orbits (see, e.g., Ref. 11).

In Section 2, the optical geometry relative to the family of locally non-rotating observers and the corresponding centrifugal force are given. In Section 3, the embedding conditions are discussed, the Kerr backgrounds are classified according to the properties of the diagrams, typical embedding diagrams are depicted, and embeddability of regions in which photon circular orbits appear is discussed. In Section 4 concluding remarks are presented.

2 Optical geometry

For definition of the optical reference geometry and the inertial forces in the Kerr backgrounds, the locally non-rotating observers (or, equivalently, zero angular momentum observers) introduced by Bardeen [12] are the most convenient, because the field of the 4-velocities of these observers is orthogonal to the $t = \mathrm{const}$ hypersurfaces [13]. The Kerr metric expressed in terms of the locally non-rotating frames (LNRF) is given by

$$ds^2 = -\frac{\Sigma\Delta}{A}\,dt^2 + \frac{\Sigma}{\Delta}\,dr^2 + \Sigma\,d\theta^2 + \frac{A\sin^2\theta}{\Sigma}\,d\hat{\phi}^2, \tag{1}$$

where

$$\Delta = r^2 - 2Mr + a^2, \tag{2}$$
$$\Sigma = r^2 + a^2\cos^2\theta, \tag{3}$$
$$A = (r^2 + a^2)^2 - a^2\Delta\sin^2\theta, \tag{4}$$
$$d\hat{\phi} = d\phi - \omega_{\mathrm{LNRF}}\,dt; \tag{5}$$

the angular velocity of the LNRF relative to distant static observers is

$$\omega_{\mathrm{LNRF}} = \frac{2aMr}{A}. \tag{6}$$

The standard Boyer-Lindquist coordinates (t, r, θ, ϕ), and the geometric units ($c = G = 1$) are used. Let M and a be the mass and the specific angular momentum of the Kerr background, respectively. For simplicity we put $M = 1$ in the following; equivalently, we use units of M.

The standard conformal $(3 + 1)$ splitting introduced in [1]

$$ds^2 = \mathrm{e}^{2\Phi}\left[-dt^2 + d\tilde{l}^2\right] \tag{7}$$

yields the line element of the optical reference geometry

$$d\tilde{l}^2 = \tilde{g}_{ik}\,dx^i dx^k, \tag{8}$$

where

$$e^{2\Phi} = -g_{tt} = \frac{\Sigma\Delta}{A} \tag{9}$$

and

$$\tilde{g}_{ik} = e^{-2\Phi}\, g_{ik}. \tag{10}$$

In the equatorial plane ($\theta = \pi/2$) we obtain

$$e^{2\Phi} = \frac{r\Delta}{r^3 + a^2 r + 2a^2}, \tag{11}$$

$$\tilde{g}_{rr} = \frac{\tilde{g}_{\theta\theta}}{\Delta} = \frac{r^4 + a^2 r^2 + 2a^2 r}{\Delta^2}, \tag{12}$$

$$\tilde{g}_{\phi\phi} = \frac{(r^3 + a^2 r + 2a^2)^2}{r^2\Delta}. \tag{13}$$

The event horizons of the Kerr spacetimes are given by the relation

$$a^2 = a^2_{\mathrm{h}}(r) \equiv r(2-r); \tag{14}$$

radii of photon circular orbits are determined by (see, e.g., Ref. 12)

$$a^2 = a^2_{\mathrm{ph}}(r) \equiv \tfrac{1}{4} r(r-3)^2. \tag{15}$$

The centrifugal force acting on a test particle moving in the equatorial plane along a $r = \mathrm{const}$ trajectory is determined by the relation (see Ref. 11)

$$F_{\mathrm{c}} = \frac{r(r^5 - 3r^4 + a^2 r^3 - 3a^2 r^2 + 6a^2 r - 2a^4)}{(r^3 + a^2 r + 2a^2)^2}\, L^2, \tag{16}$$

where L is the covariant angular momentum of the particle. The centrifugal force vanish and reverses sign at radii determined by the relation

$$a^2 = a^2_{\mathrm{c}\pm}(r) \equiv \tfrac{1}{4} r\left(r^2 - 3r + 6 \pm \sqrt{r^4 + 2r^3 - 3r^2 - 36r + 36}\right). \tag{17}$$

The maximum of the function $a^2_{\mathrm{c}+}(r)$ is located at $r_{\max(1)} = 0.81159$, where

$$a^2_{\mathrm{c}+,\max(1)} = 1.36668. \tag{18}$$

The functions $a^2_{\mathrm{h}}(r)$, $a^2_{\mathrm{ph}}(r)$, and $a^2_{\mathrm{c}\pm}(r)$ are drawn in Fig. 1. Of course, the part of the function $a^2_{\mathrm{c}-}(r)$ lying between the black-hole horizons is physically irrelevant.

3 Embedding diagrams

In order to obtain an intuitive understanding of the properties of the optical geometry (8), it is useful to embed its equatorial plane into the three-dimensional Euclidean space with the line element expressed in cylindrical coordinates as

$$ds^2 = d\rho^2 + \rho^2\, d\phi^2 + dz^2. \tag{19}$$

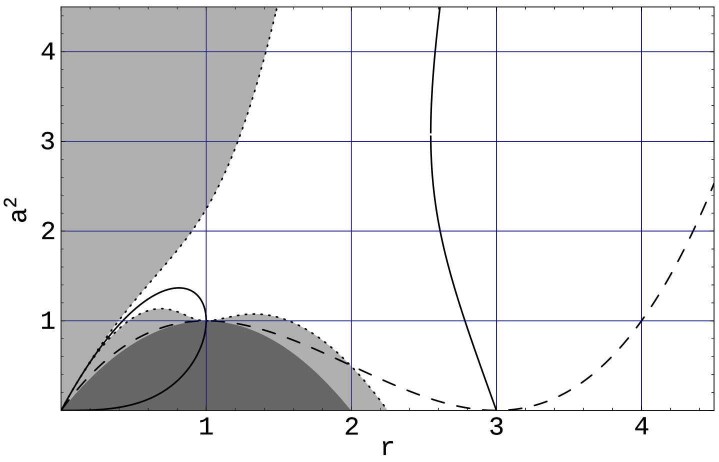

Fig. 1. Square of the specific angular momentum corresponding to the event horizons ($a^2_{\rm h}$, border between the dark gray dynamic area, where the optical geometry is not defined, and the light gray non-embeddable area), photon circular orbits ($a^2_{\rm ph}$, dashed curve), turning points of the embedding diagram ($a^2_{\rm c\pm}$, solid curve), and embeddability region border ($a^2_{\rm e}$, dotted curve enclosing the light gray area not embeddable into Euclidean space) as functions of the radius.

We have to find a surface $z = z(\rho)$ in the Euclidean space, isometric to the two-dimensional space

$$d\tilde{l}^2 = \tilde{g}_{rr}\, dr^2 + \tilde{g}_{\phi\phi}\, d\hat{\phi}^2, \tag{20}$$

with $\tilde{g}_{rr}$ and $\tilde{g}_{\phi\phi}$ given by (12) and (13). Thus, the line element (20) is to be identified with the line element

$$dl^2_{\rm (E)} = \left[1 + \left(\frac{dz}{d\rho}\right)^2\right] d\rho^2 + \rho^2\, d\phi^2. \tag{21}$$

Identifying the azimuthal coordinates ($\hat{\phi} = \phi$), the radial coordinates are related by

$$\rho^2 = \tilde{g}_{\phi\phi}. \tag{22}$$

The embedding formula $z = z(\rho)$ is determined by the relation

$$\left(\frac{dz}{d\rho}\right)^2 = \tilde{g}_{rr}\left(\frac{dr}{d\rho}\right)^2 - 1. \tag{23}$$

However, it is convenient to transfer this formula to a parametric form with r being the parameter:

$$\frac{dz}{dr} = \pm\sqrt{\frac{r^4 + a^2r^2 + 2a^2r}{(r^2 - 2r + a^2)^2} - \left(\frac{d\rho}{dr}\right)^2}. \tag{24}$$

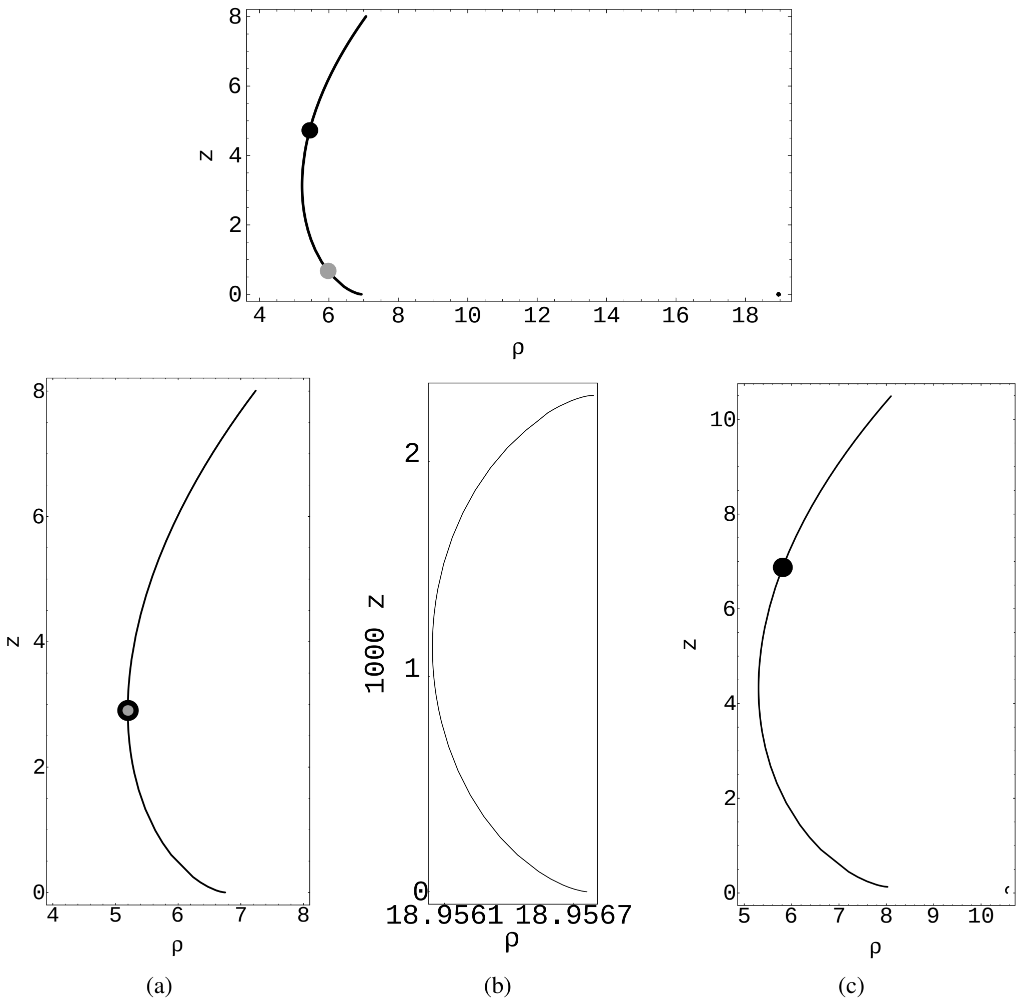

Fig. 2. Typical embedding diagram of the optical geometry of the Kerr black holes. The 1D sections are given for the three cases listed in Table 1. (a) The Schwarzschild case ($a^2 = 0$)—the gray dot inside a black ring reminds that both directions of orbiting photons have the same position. (b) The Kerr case with both the photon circular orbits being embeddable ($a^2 = 0.3$, middle top). Both corotating (gray dot) and counterrotating (black dot) photon orbits are displaced from the turning point of the diagram. The distance between different regions of embeddability has no meaning because there is no connection between them in the Euclidean space used for the embedding. Here, a 'zoom' of the embeddable part of the space under the inner horizon that appears as the small dot in the right lower corner of the top diagram is given (middle bottom). (c) The Kerr case with only counterrotating photon orbit being embeddable ($a^2 = 0.95$).

Because there is

$$\frac{dz}{d\rho} = \frac{dz}{dr}\frac{dr}{d\rho}, \tag{25}$$

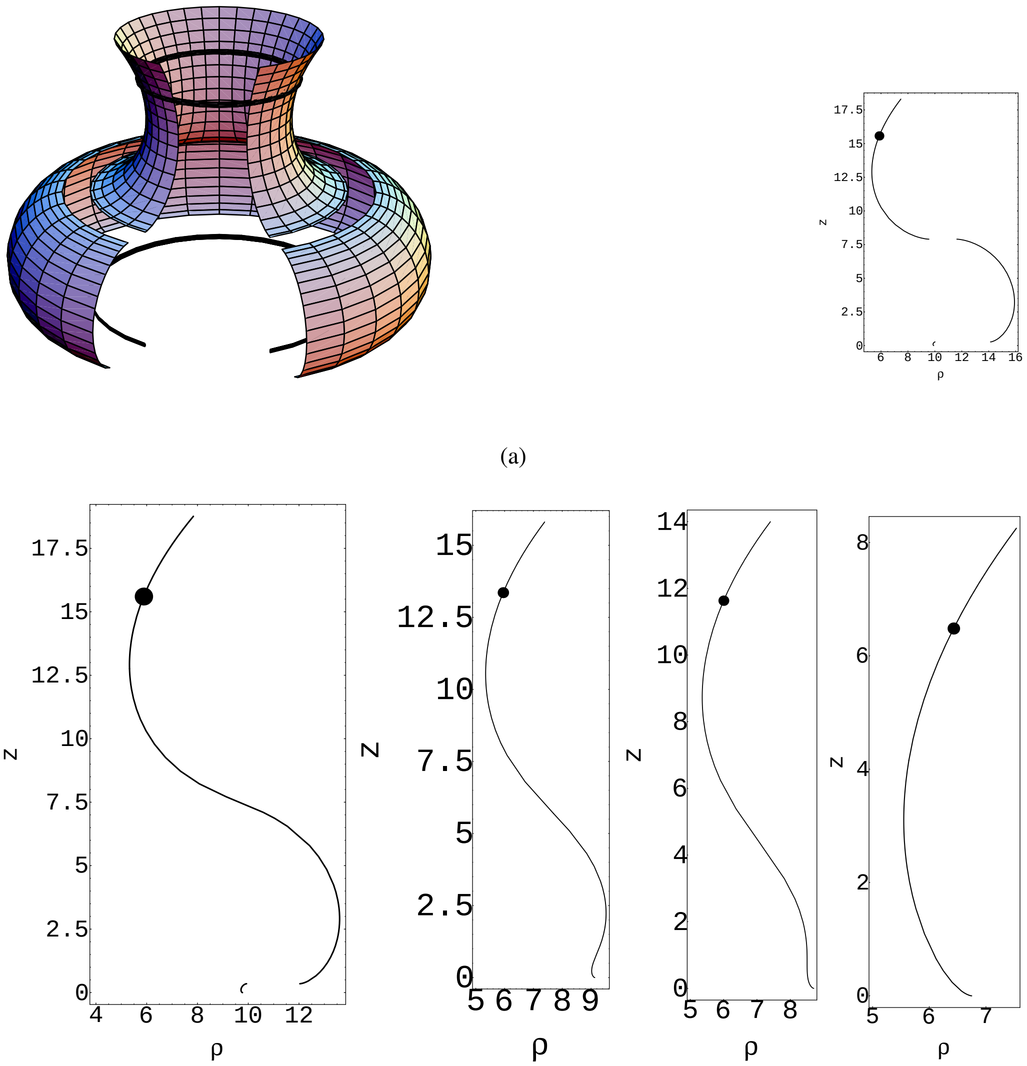

(a)

(b) (c) (d) (e)

Fig. 3. Typical embedding diagrams of the optical geometry of the Kerr naked singularities. The 1D sections are given for the five cases listed in Table 2. (a) $a^2 = 1.07$, here we include 3D picture for illustration; (b) $a^2 = 1.1$; (c) $a^2 = 1.25$; (d) $a^2 = a^2_{\mathrm{c+,max(1)}} = 1.36668$; and (e) $a^2 = 2.5 > a^2_{\mathrm{c+,max(1)}}$.

it is clear that the turning points of the embedding diagram (determining its throats and bellies) are given by the condition

$$\frac{d\rho}{dr} = 0. \tag{26}$$

Class	Interval of a^2	Description
Ia	$a^2 \leq a^2_{\rm ep} = 0.50566$	Both co- and counterrotating photon circular orbits appear on the embedding (Fig. 2 a,b)
Ib	$a^2_{\rm ep} < a^2 \leq 1$	Only counterrotating photon circular orbit lies on the embedding (Fig. 2 c)

Table 1. Classification of embedding diagrams of Kerr black holes according to embeddability of photon circular orbits.

Since

$$\frac{d\rho}{dr} = \frac{r^5 - 3r^4 + a^2r^3 - 3a^2r^2 + 6a^2r - 2a^4}{r^2(r^2 - 2r + a^2)^{3/2}}, \tag{27}$$

we immediately see that the turning points of the embedding diagram are located at radii, where the centrifugal force vanish and reverses sign. Therefore, at least one part of the properties of embeddings of the optical space of the vacuum spherically symmetric spacetimes survives—the turning points remain at radii where $F_{\rm c} = 0$. (One can understand this directly from the fact that both ρ and $F_{\rm c} \sim \tilde{g}_{\phi\phi}$.)

The embedding condition $(dz/dr)^2 \geq 0$ implies the relation

$$\begin{aligned} 4r^9 &- 9r^8 + 12a^2r^7 - 34a^2r^6 + 6a^2(2a^2+6)r^5 - 33a^4r^4 \\ &+ 4a^4(a^2+9)r^3 - 12a^4(a^2+3)r^2 + 24a^6r - 4a^8 \geq 0. \end{aligned} \tag{28}$$

This relation can be considered as quartic in a^2, nevertheless it deserves a numerical study (it is not worth to put explicitly the long expressions for the solutions of the quartic equation). The results are given by the embeddability function $a^2_{\rm e}(r)$ which is drawn in Fig. 1. The function $a^2_{\rm e}(r)$ has a local minimum $a^2_{\rm e,min} = 1$ (at $r = 1$), and two maxima, $a^2_{\rm e,max(2)} = 1.13540$ (at $r = 0.68947 < 1$), and $a^2_{\rm e,max(1)} = 1.07543$ (at $r = 1.33172 > 1$). For $a^2 = 0$ we arrive at the well known condition $r \geq \frac{9}{4}$ valid for Schwarzschild spacetimes.

Now we can directly see that in the case of black-hole spacetimes ($a^2 \leq 1$) only a very limited part of their regions lying under the inner event horizon can be embedded into the Euclidean space. The radii of photon circular orbits located under the inner horizon are always outside the embeddable region. The radii of the counterrotating (outer) photon circular orbits located above the outer horizon are in the embedded region for all black holes. However, the radii of the corotating (inner) photon circular orbits are located in the embeddable region only for black holes with parameter

$$a^2 < a^2_{\rm ep} = 0.50566. \tag{29}$$

In the limiting case of $a^2 = a^2_{\rm ep}$, the corotating photon circular orbit is located at $r_{\rm co\,(min)} = 1.99245$. For naked-singularity spacetimes, the radius of the photon circular orbit is always located in the embeddable region.

Class	Interval of a^2	Description
IIa	$1 < a^2 \leq a^2_{\mathrm{e,max(1)}} = 1.07543$	Three parts: two throats and a belly between (Fig. 3a)
IIb	$a^2_{\mathrm{e,max(1)}} < a^2 \leq a^2_{\mathrm{e,max(2)}} = 1.13540$	The upper throat joins the belly at $a^2 = a^2_{\mathrm{e,max(1)}}$ (Fig. 3b)
IIc	$a^2_{\mathrm{e,max(2)}} < a^2 < a^2_{\mathrm{c+,max(1)}} = 1.36668$	Both throats are joined by a belly (Fig. 3c)
IId	$a^2 = a^2_{\mathrm{c+,max(1)}} = 1.36668$	Special case: the belly vanish through an inflex point (Fig. 3d)
IIe	$a^2 > a^2_{\mathrm{c+,max(1)}} = 1.36668$	Only one throat remains (Fig. 3e)

Table 2. Classification of embedding diagrams of Kerr naked singularities according to the properties of the regions of embeddability.

On the other hand, the radii corresponding to the vanishing centrifugal force are always in the regions of embeddability, except the physically irrelevant radii located between the horizon (see Fig. 1).

Thus, considering the photon circular orbits, there are two classes of embedding diagrams of Kerr black holes (see Table 1). In all black-hole cases the diagram consists of two parts (the first above the outer horizon, and the second under the inner horizon), with each part having shape of a throat around the radius of the vanishing centrifugal force. The 1-dimensional sections of the embedding diagrams of black-hole spacetimes are given in Fig. 2; for comparison and completeness, the Schwarzschild case is included.

The extreme Kerr black holes ($a^2 = 1$) represent a singular situation where the embeddability condition is also satisfied just at $r = 1$. It is well known that in the ordinary space $r = 1$ represent an infinite cylinder in the proper radial coordinate including the horizon, and the corotating photon circular orbit, marginally bound and marginally stable orbit (see Ref. 12). Here, the limiting procedure from [12] cannot be used due to the fact that for all nearly extreme black holes all the orbits are located outside the embeddable region.

For Kerr naked singularities the situation is more complex although only one photon circular orbit exists in the field of naked singularities, which is always located in the embeddable region. There are five classes of naked-singularity spacetimes according to the properties of the regions of embeddability (see Table 2.). The representative embedding diagrams are given in Fig. 3.

4 Concluding remarks

We can see how the rotation parameter 'enriched' the structure of embedding diagrams of Kerr backgrounds in comparison with Schwarzschild and Reissner-Nordström backgrounds. Namely, for Kerr backgrounds the embeddings consist of two separated parts in all black-hole spacetimes, and can even contain three separated parts in naked-singularity spacetimes (if $1 < a^2 < a^2_{\mathrm{e,max(1)}} = 1.07543$), in contrast to the embeddings of the optical geometry of the Reissner-Nordström backgrounds having no separated parts (see Ref. 6). Moreover, there can exist even three turning points of the embedding diagrams of naked singularities, and there are no embeddings with no turning points, as happens for Reissner-Nordström naked singularities with charge parameter $e^2 > \frac{9}{8}M^2$.

Notice, however, that there is no evident link between the embeddability limits of Kerr backgrounds and a physical phenomenon, similar to the existence limit of static configurations of uniform density present in the spherically symmetric spacetimes. It is not clear, if the embeddability condition of Kerr spacetimes could be somehow connected to the problem of their matter sources and it stands as a challenge for future investigations.

Acknowledgements The work on this paper has been supported by grants GAČR 202/99/0261 and J10/98: 192400004, by the Committee for Collaboration of the Czech Republic with CERN, and by the Abdus Salam International Centre for Theoretical Physics in Trieste, Italy. The work had been started during authors' visit at the ICTP in Trieste, and was finished during their stay at CERN, Geneva. The authors would like to thank both ICTP and CERN for perfect hospitality and excellent conditions for work. Our special thanks are directed to Prof. Marek Abramowicz for very stimulating discussions.

References

[1] M.A. Abramowicz, B. Carter, J.P.Lasota: *Gen. Rel. Grav.* **20** (1988) 1173

[2] M.A. Abramowicz: *Monthly Notices Roy. Astron. Soc.* **256** (1992) 710

[3] M.A. Abramowicz, J.C. Miller: *Monthly Notices Roy. Astron. Soc.* **245** (1990) 729

[4] M.A. Abramowicz, J.C. Miller, Z. Stuchlíl: *Phys. Rev. D***47** (1993) 1440

[5] M.A. Abramowicz, A.R. Prasanna: *Monthly Notices Roy. Astron. Soc.* **245** (1990) 720

[6] S. Kristiansson, S. Sonego, M.A. Abramowicz: *Gen. Rel. Grav.* **30** (1998) 275

[7] Z. Stuchlík: *Bull. Astron. Inst. Czechosl.* **41** (1990) 341

[8] Z. Stuchlík, S. Hledík: *Class. Quantum Grav.* **16** (1999) 1377

[9] Z. Stuchlík, S. Hledík: *to appear in Phys. Rev. D.*

[10] Z. Stuchlík: *preprint TPA 007, Silesian University.*

[11] S. Iyer, and A.R. Prasanna: *Class. Quantum Grav.* **10** (1993) L13.

[12] J.M. Bardeen: In *Black Holes*, C. De Witt and B. S. De Witt, eds. (Gordon and Breach, New York-London-Paris, (1973) p. 215.

[13] M.A. Abramowicz, P. Nurowski, N. Wex: *Class. Quantum Grav.* **12** (1995) 1467